Effect of Fluid Motion on Free Surface Shape under Reduced Gravity

JIN H. CHIN* AND L. W. GALLAGHER†
Lockheed Missiles and Space Company, Sunnyvale, Calif.

UNDER reduced gravity conditions, the free-surface shape of a liquid propellant in a tank may be highly curved. Under static conditions, the free-surface shape is determined by the balance between surface tension forces and gravity forces. When fluid motion exists, whether caused by effects of buoyant forces or by surface-tension gradient, the free surface may change from its static shape. Since the energy transfer across the free surface and between the propellant and tank wall depends upon the free-surface shape and the wetted area, it is of both theoretical and practical interest to examine the fluid-motion effects on free-surface shape under reduced gravity conditions.

The fluid motion under the conditions of interest is governed by the usual conservation equations in fluid dynamics. The main difference is in the boundary conditions at the free surface. However, the system of equations with the boundary conditions is complex and highly "coupled"; its solution is difficult without many simplifications and approximations. In this study, the fluid motion effects will be examined qualitatively by solving an "uncoupled" problem; that is, the free-surface shape will be calculated by assuming that the free surface is an axisymmetric stream surface with given axisymmetric velocity distributions.

The conditions along a stream surface may be described by Bernoulli's equation:

$$p + (\rho g y/g_c) + (\rho u^2/2g_c) = p_0 \tag{1}$$

where on the left-hand side are the pressure, gravity, and velocity heads, respectively, for a point on the liquid side of the free surface at radial distance r; p_0 is the pressure head at the origin. From a symmetry consideration, the stream velocity at the origin vanishes. The g field is assumed to be in the negative $-y$ or axial direction.

Because of the free-surface curvature, a difference exists between the liquid pressure p and the ullage pressure p_g:

$$p_g - p = \frac{\sigma}{r}\left[\frac{ry_r}{(1 + y_r^2)^{1/2}}\right]_r \tag{2}$$

where σ is the liquid surface tension, and the subscript r means differentiation with respect to r. Equation (2) reduces to the Laplace equation when the free-surface shape is spherical. Since the ullage pressure is uniform, Eqs. (1) and (2) may be combined to yield

$$\frac{\sigma}{r}\left[\frac{ry_r}{(1 + y_r^2)^{1/2}}\right]_r - \frac{\rho g y}{g_c} - \frac{\rho u^2}{2g_c} - 2\sigma y_{rr}(0) = 0 \tag{3}$$

where the last term is obtained by evaluating the first term at $r = 0$, with the condition of symmetry $y_r(0) = 0$ and using the L'Hospital rule. Now Eq. (3) may be nondimensionalized by introducing $F = y/a$, $R = r/a$, and $V = u/u_m$, where a is the tank radius and u_m the maximum free-surface velocity; that is,

$$\frac{1}{R}\left[\frac{R\,F_R}{(1 + F_R^2)^{1/2}}\right]_R - BF - \frac{W}{2}V^2 - 2F_{RR}(0) = 0 \tag{4}$$

where $B = \rho g a^2/\sigma g_c$ = Bond number, and $W = \rho a u_m^2/\sigma g_c$ = Weber number. Equation (4) is a second-order, nonlinear, ordinary differential equation with the following boundary conditions: $F_R(0) = 0$, condition of symmetry; $F_R(1) = \cot\theta$, condition of satisfaction of contact angle. Before solution $F_{RR}(0)$ is not known; its value must be such to satisfy the two boundary conditions and the datum condition $F(0) = 0$. Without solving the "coupled" problem, the selection of the velocity distribution is somewhat arbitrary. In addition to the symmetry condition $V(0) = 0$ already mentioned, the no-slip condition $V(1) = 0$ may be used. From the consideration of liquid stratification in a tank, the flow near the free-surface center may be similar to an "inverted" axisymmetric stagnation flow with a tangential velocity proportional to the radial distance. The flow near the side wall is more complicated and is likely to be "separated" near the "corner" region. If separation does not occur, then the flow near the side wall may be similar to one-half of an "inverted," oblique, two-dimensional impinging jet. As a first approximation, the "approach" velocity toward the wall along the stagnation streamline in the jet is proportional to the distance from the wall. One of the simplest velocity distributions that satisfies the preceding behaviors is a double-sine distribution given by

$$V = \begin{cases} \sin\dfrac{\pi}{2}\left(\dfrac{R}{R_m}\right) & 0 \le R \le R_m \\ \sin\dfrac{\pi}{2}\left(\dfrac{1 - R}{1 - R_m}\right) & R_m \le R \le 1 \end{cases} \tag{5}$$

where R_m is the radial location of u_m. This velocity distribution will be used for the numerical calculations.

The magnitude of the Bond number depends on the liquid properties, tank radius, and the g level. For instance, $B = 2$ for liquid hydrogen, $a = 10$ ft, and $g/g_0 = 10^{-6}$. The magnitude of the Weber number is more difficult to determine. From order-of-magnitude considerations of the effects of side-wall free convection and surface-tension gradient, Chin[1] shows that, at low g levels, the Weber number can be very large. For instance, $W \backsim 10$ for liquid hydrogen, $a = 10$ ft, $g/g_0 = 10^{-6}$, side-wall heat flux = 1 Btu/ft²-hr, and propellant height = 10 ft. However, with the mathematical model used, and for a given Bond number, contact angle, and velocity distribution, there exists a limiting Weber number above which numerical solutions cannot be obtained ($F_R = \infty$ for $R < 1$). Thus, the range of the Weber number of interest is not unlimited.

For small values of B, Eq. (4) may be solved numerically by the method of integral and successive approximations. After each term of Eq. (4) is multiplied by RdR and then integrated from $R = 0$ to $R = R$, the following equation is obtained:

$$\frac{R\,F_R}{(1 + F_R^2)^{1/2}} = F_{RR}(0)R^2 + \frac{W}{2}\int_0^R V^2 R dR + B\int_0^R F R dR \tag{6}$$

The factor $F_{RR}(0)$ may be eliminated by applying the boundary condition at $R = 1$ to Eq. (6). After manipulations, there results

$$R\,F_R/(1 + F_R^2)^{1/2} = E(R) \tag{7}$$

where

$$E(R) = R^2\cos\theta + \frac{W}{2}\left(\int_0^R V^2 R dR - R^2\int_0^1 V^2 R dR\right) + B\left(\int_0^R F R dR - R^2\int_0^1 F R dR\right)$$

Received July 13, 1964. This work was sponsored by NASA under Contract NAS 8-11525.

* Member of Flight Technology, Research and Development Division. Member AIAA.

† Member of Flight Technology, Research and Development Division.

Equation (7) may be solved for F_R and then integrated to yield

$$F = \int_0^R \frac{E(R)dR}{[R^2 - E^2(R)]^{1/2}} \tag{8}$$

Equation (8) is an integral equation for F and may be solved by the method of successive approximations. For $B = 0$, no successive approximation is required. For small values of Bond numbers and Weber numbers ($B < 10$, $W < 5$), experience indicates that the convergence in the computer calculation is very rapid. For large values of B and W, instability is encountered during consecutive approximations; therefore, an alternate numerical method is more appropriate for these cases.

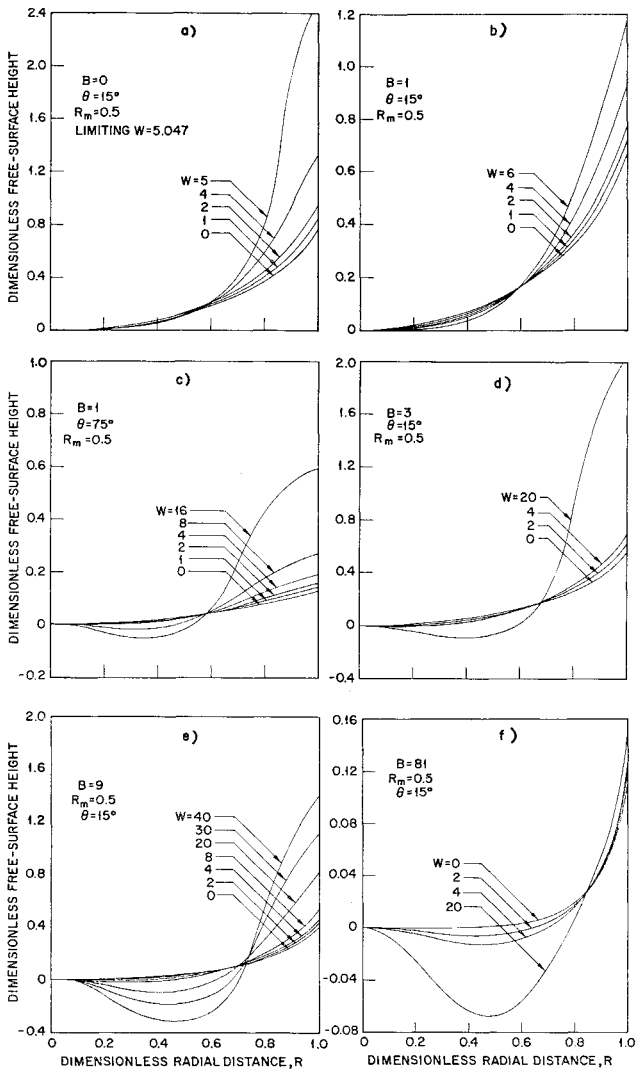

Fig. 1 Dimensionless distribution of free-surface height.

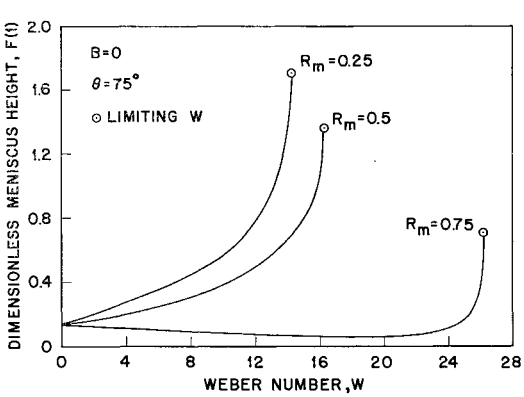

Fig. 2 Effects of Weber number and location of velocity maximum on dimensionless meniscus height.

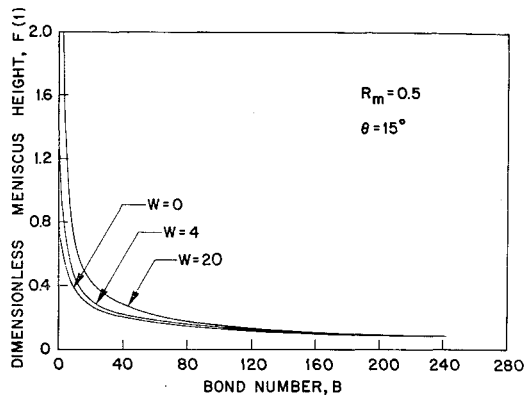

Fig. 3 Effects of Bond number and Weber number on dimensionless meniscus height.

The fact that a limiting Weber number exists in the numerical solution may be easily observed from Eq. (8) for $B = 0$; it corresponds to the smallest value of W to make $R \pm E(R) = 0$.

Expressions for some limiting cases may be obtained from Eq. (8). For instance, when $B = W = 0$, Eq. (8) yields

$$F = (1/\cos\theta)\,[1 - (1 - R^2\cos^2\theta)^{1/2}] \tag{9}$$

which is an equation for a circle. For $B \ll 1$ and $W = 0$, Eqs. (8) and (9) may be used to yield a first-order approximation for F:

$$F \approx \frac{1}{\cos\theta}\,[1 - (1 - R^2\cos^2\theta)^{1/2}] - \frac{B}{3\cos^3\theta}\left\{\ln\frac{2}{[1 + (1 - R^2\cos^2\theta)^{1/2}]} + \frac{R^2}{2}\cos^2\theta - \left(\frac{1 + \sin\theta + \sin^2\theta}{1 + \sin\theta}\right)[1 - (1 - R^2\cos^2\theta)^{1/2}]\right\} \tag{10}$$

An alternate numerical method using the Runge-Kutta technique of solving Eq. (4) is used, involving the iteration of the values of $F_{RR}(0)$ to satisfy the correct value of θ. One nonlinear characteristic of Eq. (4) is that F_R may change from a small number to a very large number in one integration step, if the initially assumed $F_{RR}(0)$ is not near the correct value. To prevent computer overflow, the integration process is stopped whenever $|F_R| > 10^7$ and the iteration cycle is continued with a more appropriate value of $F_{RR}(0)$. The convergence of the numerical solution is rapid for all Bond numbers, provided that the Weber number is less than the limiting value.

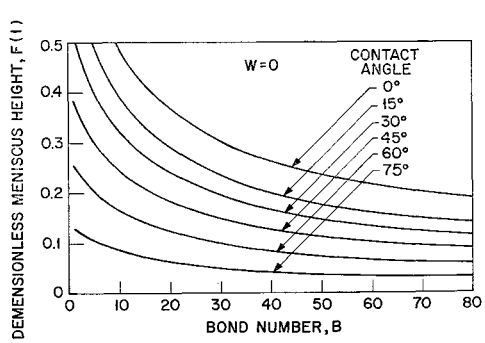

Fig. 4 Effects of Bond number and contact angle on dimensionless meniscus height.

Figures 1a–1f show the dimensionless distribution of free-surface height for $R_m = 0.5$ and different values of B. The effects of the contact angle θ may be seen by comparison of Figs. 1b and 1c. The effects of Weber number on the dimensionless meniscus height $F(1)$ are shown in Fig. 2 for different values of R_m; the limiting Weber numbers are also indicated. Figure 3 shows the effects of Bond numbers on the meniscus height for $\theta = 15°$, $R_m = 0.5$, and different values of W. The meniscus heights for the static case are given in Fig. 4.

The following conclusions may be drawn from Figs. 1–4: 1) surface velocities have strong effects on liquid free-surface shape and meniscus height; 2) the relative effect of Weber number on the meniscus height decreases as the Bond number increases; and 3) for the velocity distributions selected, the meniscus height increases for most cases as the Weber number is increased (there are exceptions, e.g., for the case with $B = 0$, $\theta = 75°$, and $R_m = 0.75$).

Reference

[1] Chin, J. H., et al., "Theoretical and experimental studies of zero-g heat transfer modes," Lockheed Missiles and Space Co., Monthly Progr. Rept., NASA Contract NAS 8-11525 (November–December 1963).

Influence of Magnetic Fields upon Separation

WILLIAM H. HEISER*
Massachusetts Institute of Technology, Cambridge, Mass.

IT is well known that rotational motion of a conductor is resisted by induced currents if a magnetic field not parallel to the axis of rotation is applied. For example, a solid cylindrical shell of arbitrary thickness and diameter set spinning initially with angular velocity ω_0 in the presence of a transverse magnetic field B_0 (Fig. 1) can be shown to slow down in accordance with the equation

$$\omega(t) = \omega_0 \exp\{-(\sigma B_0^2/2\rho)t\}$$

provided that ρ and σ are constant throughout the material, $D_0 \ll H$, and $\mu_0\sigma\omega_0 D_0^2$ (the magnetic Reynolds number) $\ll 1$. The striking magnitude of this effect is indicated by the result that the time required for a copper shell to slow to $\frac{1}{10}$ of its initial rotational speed ($4.6\rho/\sigma B_0^2$) in the presence of a transverse field of 1 w/m^2 is only $\sim 10^{-3}$ sec. The resistance to radial current flow causes the decay time to increase as D_0/H increases.

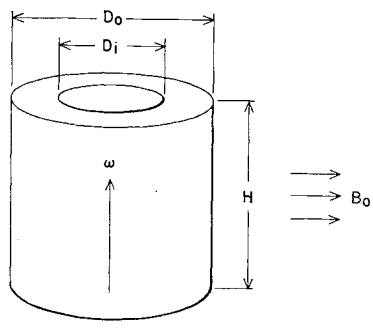

Fig. 1 Solid cylindrical shell spinning in transverse magnetic field.

Received July 16, 1964. These experiments were performed for the film "Magnetohydrodynamics" by J. A. Shercliff, produced by Educational Services Inc. for the National Committee for Fluid Mechanics Films, with the financial support of the National Science Foundation.

* Assistant Professor of Mechanical Engineering.

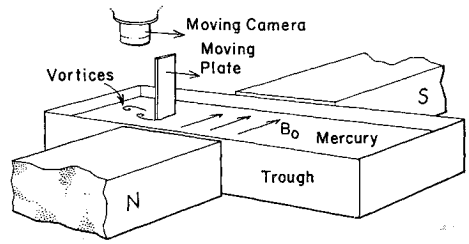

Fig. 2 Schematic representation of the experiment.

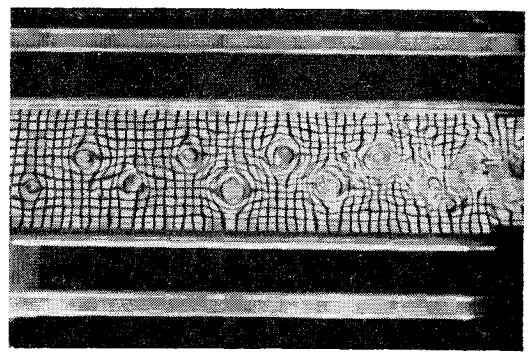

Fig. 3 Vortex street generated in the magnetic field-free region at the start of the run.

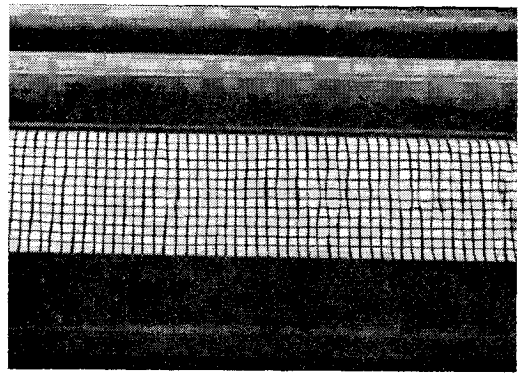

Fig. 4 No vortex street can be observed within the region of transverse magnetic field.

Experiments were conducted to demonstrate this effect upon the Kármán vortex street generated by a flat plate moving with constant velocity through still mercury (Fig. 2) at the studios of Educational Services Inc., Watertown, Mass. The experiments were photographed from above as a grid, with an apparent spacing approximately the diameter of the individual vortices, was reflected from the mercury surface. This technique made the small surface dimples caused by the rotating mercury quite visible as distortions of the regular grid pattern.

Figures 3–5 are three consecutive photographs of the reflected grid pattern taken during a single constant velocity run from left to right, the flat plate being at the extreme right in each photograph. Figure 3 shows clearly the vortex street generated outside the region of transverse magnetic field. Figure 4 gives no indication that vortices are ever generated within the region of magnetic field. Figure 5 shows the resumption of the vortex street in the region where the magnetic field fringes. For the experiment shown in